A&A 625, A78 (2019)
https://doi.org/10.1051/0004-6361/201935101

Astronomy & Astrophysics

Excitation and charge transfer in low-energy hydrogen atom collisions with neutral carbon and nitrogen⋆

A. M. Amarsi[1] and P. S. Barklem[2]

[1] Max Planck Institute für Astronomy, Königstuhl 17, 69117 Heidelberg, Germany
e-mail: amarsi@mpia.de
[2] Theoretical Astrophysics, Department of Physics and Astronomy, Uppsala University, Box 516, 751 20 Uppsala, Sweden
e-mail: paul.barklem@physics.uu.se

Received 22 January 2019 / Accepted 30 March 2019

ABSTRACT

Low-energy inelastic collisions with neutral hydrogen atoms are important processes in stellar atmospheres, and a persistent source of uncertainty in non-LTE modelling of stellar spectra. We have calculated and studied excitation and charge transfer of C I and of N I due to such collisions. We used a previously presented method that is based on an asymptotic two-electron linear combination of atomic orbitals (LCAO) model of ionic-covalent interactions for the adiabatic potential energies, combined with the multichannel Landau-Zener model for the collision dynamics. We find that charge transfer processes typically lead to much larger rate coefficients than excitation processes do, consistent with studies of other atomic species. Two-electron processes were considered and lead to non-zero rate coefficients that can potentially impact statistical equilibrium calculations. However, they were included in the model in an approximate way, via an estimate for the two-electron coupling that was presented earlier in the literature: the validity of these data should be checked in a future work.

Key words. atomic data – atomic processes – line: formation – radiative transfer – stars: abundances

1. Introduction

Carbon and nitrogen, respectively the second and fourth most abundant metals in the Sun, are among the most important elements in modern astrophysics. They play a key role in stellar physics as catalysts in the CNO-cycle. As a result of this cycle their abundances are interlinked, and their abundances in the surfaces of stars that have dredged-up or mixed C-poor, N-rich material from the interior has been used to study stellar evolution (e.g. Gratton et al. 2000; Spite et al. 2005). Since the amount of mixing is sensitive to stellar mass, [C/N] measurements are also good indicators of the ages of late-type giants (e.g. Masseron & Gilmore 2015; Salaris et al. 2015; Martig et al. 2016). Finally, C-N abundance variations in globular cluster stars of the same evolutionary stages shed light on their formation histories and different populations (e.g. Gratton et al. 2012).

As such, it is highly desirable to determine carbon and nitrogen abundances as accurately as possible. Lines of C I and N I are commonly used to measure carbon and nitrogen abundances, in the Sun (e.g. Asplund et al. 2009; Caffau et al. 2009, 2010) and early- and late-type stars (e.g. Tomkin & Lambert 1978; Clegg et al. 1981; Takeda 1994; Przybilla et al. 2001; Przybilla & Butler 2001; Shi et al. 2002; Takeda & Honda 2005; Lyubimkov et al. 2011, 2015).

It is well-known that the formation of C I and N I lines in stellar atmospheres is sensitive to departures from local thermodynamic equilibrium (LTE). Non-LTE modelling requires a complete description of all the relevant radiative and collisional bound-bound and bound-free transitions, and historically the lack of reliable data for inelastic collisions with electrons and with hydrogen has been a dominant source of uncertainty. The situation has recently improved for C I and N I, for which recent *B*-spline *R*-matrix (BSR) calculations have put the rates of electron-impact excitation and ionisation on firmer footing (Wang et al. 2013, 2014).

Concerning inelastic collisions with neutral hydrogen, full quantum-scattering calculations within the Born-Oppenheimer approach for Li I, Na I, and Mg I have indicated the importance of excitation and charge transfer through avoided ionic crossings (Belyaev et al. 1999, 2010, 2012; Belyaev & Barklem 2003; Guitou et al. 2011). As discussed in previous papers in this series (Barklem 2018a,b), such calculations are time-consuming and complicated. As a result, several asymptotic methods have been developed to model this mechanism: namely, the methods of Belyaev (2013) based on semi-empirical couplings (Olson et al. 1971); and of Barklem (2016a), with theoretical couplings derived from a theoretical two-electron linear combination of atomic orbitals (LCAO; Grice & Herschbach 1974; Adelman & Herschbach 1977). These asymptotic methods reproduce the full quantum scattering results reasonably well, at least for for the species Li I, Na I, and Mg I and for processes involving states of low excitation potential having large rate coefficients (that tend to be of importance for statistical equilibrium calculations involving these species).

Here, we present calculations for inelastic collisions with neutral hydrogen using the LCAO model of Barklem (2016a), for C I and N I. We present the method in Sect. 2, and discuss the

⋆ Atomic data are available at the CDS via anonymous ftp to cdsarc.u-strasbg.fr (130.79.128.5) or via http://cdsarc.u-strasbg.fr/viz-bin/qcat?J/A+A/625/A78 and at https://github.com/barklem/public-data

results of the calculations in Sect. 3. We summarise these data and remark on their applicability in Sect. 4.

2. Method

2.1. Input data and assumptions

Calculations of the transitions through avoided ionic crossings (via the $C^+ + H^-$ and $N^+ + H^-$ ionic configurations) were performed following the method described in Barklem (2016b), where it is applied to Li I, Na I, Mg I, and Ca I. The method was subsequently applied to O I (Barklem 2018b), Fe I (Barklem 2018a), as well as K I and Rb I (Yakovleva et al. 2018). As in those works, the production runs were based on adiabatic potential energies and coupling parameters derived from the LCAO model. The potential energies were calculated for internuclear distances $3.0 \leq R/a_0 \leq 400.0$: at shorter internuclear distances, other couplings not considered here (rotational and spin-orbit couplings) are likely to be important, while avoided ionic crossings at larger internuclear distances do not give rise to large rate coefficients. The collisional cross-sections were calculated using the multichannel Landau-Zener model, for collision energies from threshold up to 100 eV, from which rate coefficients were calculated for temperatures $1000 \leq T/K \leq 20\,000$.

We present the input data and the considered symmetries in Appendix A. To summarise, the energies for these low-lying levels were taken from Moore (1993) via the NIST Atomic Spectra Database (Kramida et al. 2015). Fine structure was collapsed and g-weighted energies were adopted. Ionic states involving C^+ $2p\,^2P^o$, and N^+ $2p^2\,^3P$ and N^+ $2p^2\,^1D$, were included for carbon and nitrogen respectively. Initially we had considered a greater number of ionic states, however the corresponding transitions have avoided ionic crossings at very short internuclear distances, and have a negligible impact on the current model. As a consequence of omitting some ionic states, the coefficients of fractional parentage here do not always satisfy the normalisation condition $\sum[(G^{S_C,L_C}_{S_A,L_A})^2] = 1$, summing over cores C.

Following Barklem (2018b), two-electron processes were included in an approximate way, by calculating the analogous one-electron couplings and applying a scaling factor to it based on the internuclear distance, following Eq. (1) of Belyaev & Voronov (2017) (see also earlier work by Belyaev 1993; Yakovleva et al. 2016). Two-electron processes involving hydrogen in the first excited state (energy of 10.20 eV) were considered potentially important, given the high ionisation limits of C I (ionisation limit of 11.26 eV) and N I (ionisation limit of 14.53 eV). They were considered for the $2s^2.2p^2\,^3P$ ground state of C I, and for the $2s^2.2p^3\,^4S^o$ ground state and $2s^2.2p^3\,^2D^o$ (energy of 2.38 eV) first excited state of N I. These proceed via interaction of ionic states $X^+\,2s^2.2p^a + H^-$, with covalent states $2s^2.2p^{a+1} + H\,(n = 2)$. In the current model these are interpreted as two-electron processes, wherein the two electrons initially located on H^- transfer onto X^+, and then, due to the lack of an accepting state, one transfers back, resulting in $H\,(n = 2)$.

Two-electron processes with hydrogen in its ground state were also considered, for the $2s.2p^3$ configurations of C I, and for the $2s.2p^4$ configuration of N I. These proceed via interaction of ionic states $X^+\,2s^2.2p^a + H^-$, with covalent states $2s.2p^{a+2} + H\,(n = 1)$[1]. These processes present added complications. The assumption implicit in the model, that the core is in a frozen configuration, breaks down. As a result, the angular momentum coupling term, C in Eqs. (19) and (20) of Barklem (2016a), usually calculated for one particular frozen core, is here undefined, as is the electron binding energy and the coefficient of fractional parentage. To be able to obtain some estimate with the existing model, a number of approximations were made for the covalent states: namely, the angular momentum coupling terms were set to unity, the electron binding energies were chosen to correspond to the core for which the coefficient of fractional parentage was largest, and the coefficients of fractional parentage were set to unity. The resulting rate coefficients may be considered indicative of the potential for such processes to be of significance.

[1] Hereafter, it is implied that H is in its ground state, unless otherwise indicated.

2.2. Alternative ionic channels

Only transitions via the $C^+ + H^-$ (asymptotic limit at 10.6 eV relative to the neutral ground states) and $N^+ + H^-$ (13.8 eV) ionic configurations were considered here. Other ionic configurations and channels are also possible. In particular, since C I and N I have large ionisation potentials, comparable to that of H I, transitions could occur via the $C^- + H^+$ (12.3 eV) and $N^- + H^+$ (13.7 eV) ionic configurations. We note that unless the carbon or nitrogen atom in the covalent state is in the ground configuration ($2p^2$ or $2p^3$, respectively), this interaction must involve two active electrons. For example, if the electron on the carbon atom is in the 3s orbital, then the process would involve both the transition of this electron from the 3s orbital to the 2p orbital, and in addition the transfer of the electron from the hydrogen atom to the 2p carbon core, so as to form C^- ($2p^3$). The approximate scaling factor mentioned in Sect. 2.1 is probably not appropriate in this case, because the electron is here transferring to the carbon atom in the covalent state, rather than from it, and the carbon atom undergoes rearrangement of the core electrons.

The possible importance of these alternative ionic configurations and channels was tested for carbon. Mutual neutralisation cross-sections into the ground configurations from $C^+ + H^-$ and $C^- + H^+$ were estimated using the two channel Landau Zener model together with semi-empirical couplings from Olson et al. (1971), for energies in the range 0.1–1.0 eV. The cross-sections from $C^+ + H^-$ are two orders of magnitude larger than from $C^- + H^+$ at 1.0 eV, reaching four orders of magnitude at 0.1 eV. This is understandable from the fact that the crossings for $C^- + H^+$ occur at shorter internuclear distances than for $C^+ + H^-$, as well as the binding energies of C^- and H (the initial and final states of the active electron in the former case) being larger than for H^- and C (the initial and final states of the active electron in the latter case). Thus, this estimate, combined with the expectation that the cases involving two-electron processes will generally be less efficient than the cases involving one-electron processes, suggests that $C^+ + H^-$ is unlikely to be important compared to $C^- + H^+$ at collision energies of interest.

The case of nitrogen is complicated by the fact that N^- has a negative electron affinity (−0.07 eV), and thus the assignment of the binding energy of the active electron – required to derive the semi-empirical coupling – is not obvious. The ionic crossings for $N^- + H^+$ take place at slightly larger internuclear distance than for $N^+ + H^-$. However, the expectation that the cases involving two-electron processes are generally less efficient than the cases involving one-electron processes still applies.

In summary, the $C^- + H^+$ and $N^- + H^+$ configurations were neglected in these calculations. These alternative channels are expected to be of lesser importance, however their possible influence perhaps makes these calculations somewhat more

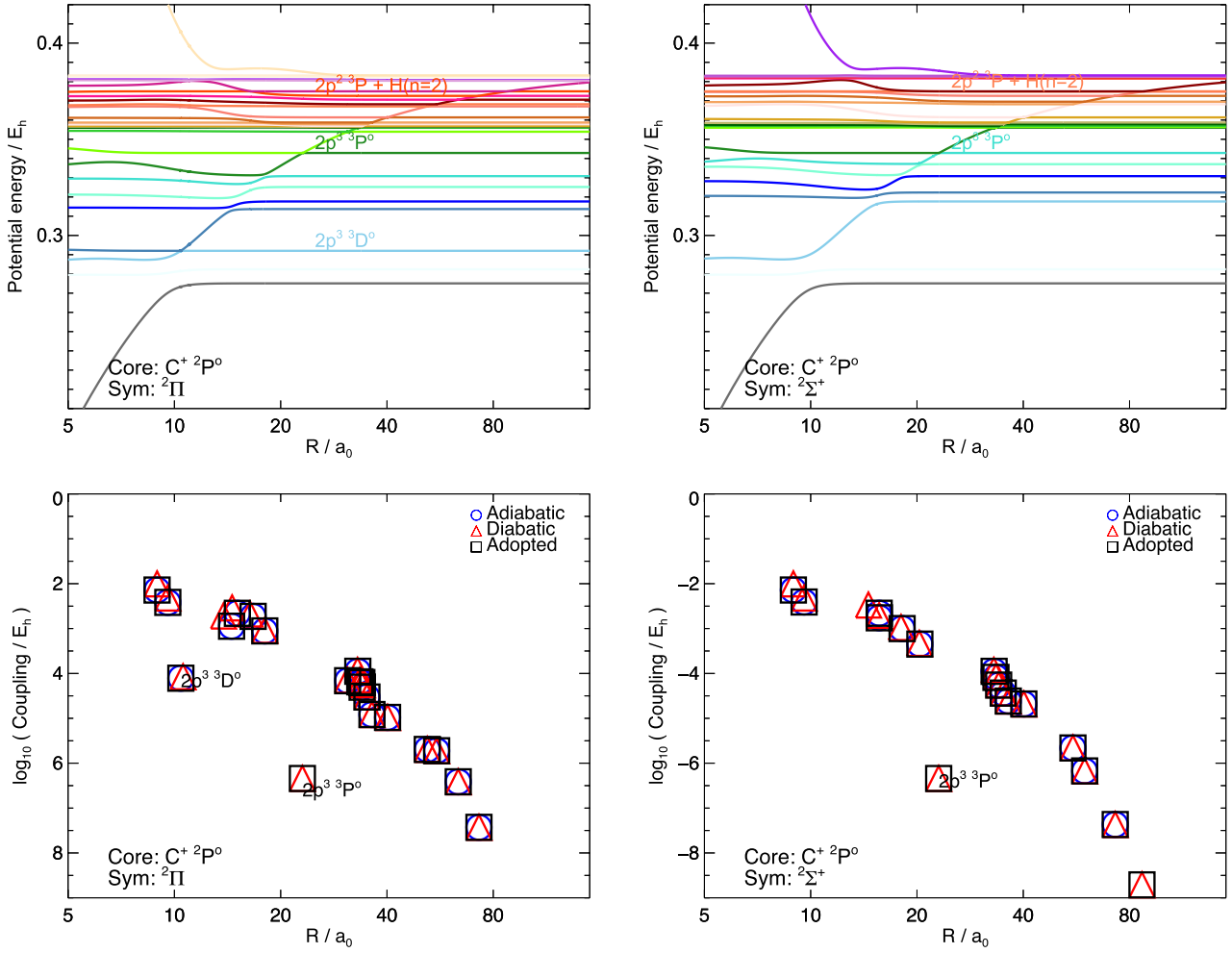

Fig. 1. Adiabatic potential energies as a function of internuclear distance (*top*), and corresponding couplings at the crossing radius (*bottom*), in atomic units (Hartree energy E_h and Bohr radius a_0, respectively), for symmetries involving the ground state ionic cores of carbon. States included in the model via two-electron processes have been labelled. The lowest-lying states have been truncated from the upper plots. For the C I $2s.2p^3\ ^3P^o$ state, the coupling is very small; the diabatic value was judged to be more reliable and the adiabatic value is not shown.

uncertain, compared to calculations for atoms with small ionisation potentials relative to that of H I. Quantum chemistry calculations would be useful to investigate the influence of these ionic configurations.

3. Results

3.1. Potentials and couplings

In the top rows of Figs. 1 and 2 we illustrate the adiabatic potential energies as a function of internuclear distance, for covalent states involving the ground state ionic cores of C II and N II. First, we note that the covalent states involving ground-state hydrogen and the four lowest-lying levels of C I ($2s^2.2p^2\ ^3P/^1D/^1S$, and $2s.2p^3\ ^5S^o$), and the three lowest-lying levels of N I ($2s^2.2p^3\ ^4S^o, ^2D^o, ^2P^o$), do not have any avoided ionic crossings in the current model, for $R \geq 3\,a_0$. Their adiabatic potential energies are not shown in the figures, lying below the horizontal axes. The plots show the covalent states involving ground-state hydrogen, and levels of intermediate and high excitation potential of C I and N I, namely C I $2s^2.2p.3s\ ^3P^o$ and N I $2s^2.2p^2.3s\ ^4P$, and higher. These have avoided ionic crossings at intermediate internuclear distances.

The top rows of Figs. 1 and 2 also show the adiabatic potential energies of the covalent states involving excited hydrogen and the lowest energy state of C I, as well as excited hydrogen and the two lowest energy states of N I. The former (C I) is relatively highly excited, and as such has its avoided ionic crossing at larger internuclear distance (close to $80\,a_0$). The latter two (N I) have avoided ionic crossings at short and intermediate internuclear distances (around $7\,a_0$ and $20\,a_0$, respectively).

In the bottom rows of Figs. 1 and 2 we illustrate the corresponding ionic-covalent coupling coefficients, calculated using both adiabatic and diabatic potential energies in the Landau-Zener formalism. As discussed in Sect. II.B.3 of Barklem (2016a), the adiabatic values are generally expected to be most reliable. However, when the couplings are very small, they are difficult to accurately determine from the potentials in the adiabatic representation, and the minimum coupling that can be resolved at a given internuclear distance is limited by the numerical properties of the calculations. In earlier work, this has only occurred for crossings at large internuclear distances and so was dealt with by adopting diabatic values at $R > 50\,a_0$. In this work, small couplings also occur at intermediate internuclear distances, for two-electron processes (for example, for the N I $2s^2.2p^3\ ^2D^o$ state in Fig. 2). In cases in which a reliable adiabatic value cannot be obtained, the diabatic values were adopted.

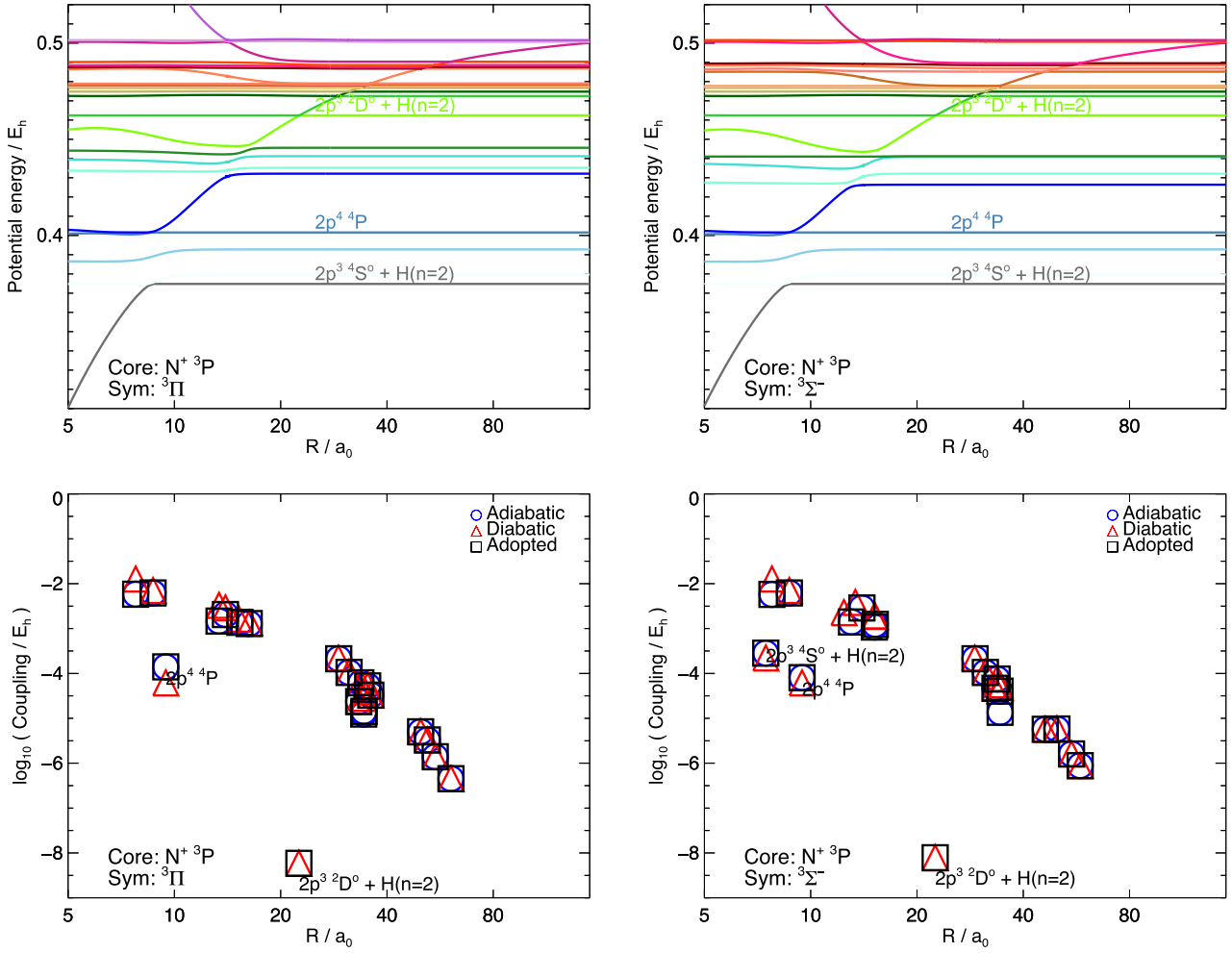

Fig. 2. Adiabatic potential energies as a function of internuclear distance (*top*), and corresponding couplings at the crossing radius (*bottom*), in atomic units (Hartree energy E_h and Bohr radius a_0, respectively), for symmetries involving the ground state ionic cores of nitrogen. States included in the model via two-electron processes have been labelled. The lowest-lying states have been truncated from the upper plots. For the N I $2s^2.2p^3\ ^2D^o + H\,(n = 2)$ state the coupling is very small; the diabatic value was judged to be more reliable and the adiabatic value is not shown.

3.2. Rate coefficients

In Figs. 3 and 4 we illustrate the resulting total rate coefficients at 6000 K. The rates are in matrix form: the lower diagonal represents downwards processes (de-excitation and mutual neutralisation), and the upper diagonal represents upwards processes (excitation and ion pair production). In Fig. 5 we plot the downwards rate coefficients as functions of the logarithm of the transition energy ΔE.

The rate coefficients are correlated with the excitation potential. The largest rates tend to involve states of intermediate and moderately-high excitation potential: for excitation and de-excitation, this corresponds to the squares in the middle of Figs. 3 and 4, while for ion pair production and mutual neutralisation, this corresponds to the squares in the middle of the last rows and columns of these figures. The rate coefficients for transitions involving the states of lowest excitation potential (shown on the first four rows and columns of Fig. 3 and the first three rows and columns of Fig. 4) are zero. As discussed in Sect. 3.1, the corresponding avoided ionic crossings happen at very short internuclear distances, beyond the regime of the present model and consequently do not give rise to any couplings. On the other hand, for the states of highest excitation potential, the rate coefficients for excitation as well as charge transfer are generally small ($\langle \sigma v \rangle < 10^{-13}\,\mathrm{cm^3\,s^{-1}}$), if not zero. The corresponding avoided ionic crossings happen at large internuclear distances, giving rise to smaller couplings: in the quantum tunnelling interpretation, this can be interpreted as a result of the electron tunnelling probability dropping off with increasing width of the potential barrier.

The rates also have a strong dependence on the transition energy. The mutual neutralisation rates in Fig. 5 have a sharp peak at around $\log(\Delta E/\mathrm{eV}) \approx 0.3$, or transition energies of around 2 eV; the de-excitation rates have a broader peak, at around $\log(\Delta E/\mathrm{eV}) \approx 0$, or transition energies of around 1 eV. In the case of de-excitation, some structure in the rate coefficients is clearly visible, generally reflecting their dependence also on the excitation potential as discussed above. This behaviour – the rate coefficients peaking at particular energies – has been previously noted in the context of other species (e.g. Barklem 2018a), and is exploited for calculating more simplified models for inelastic hydrogen collisions (e.g. Belyaev & Yakovleva 2017; Ezzeddine et al. 2018).

Charge transfer processes typically give the largest rates, as has been found in previous studies of other species. This can be seen from the dark squares in the last rows and columns of Figs. 3 and 4, and from the spike in mutual neutralisation rate coefficients at $\log(\Delta E/\mathrm{eV}) \approx 0.3$ in Fig. 5. This result can be

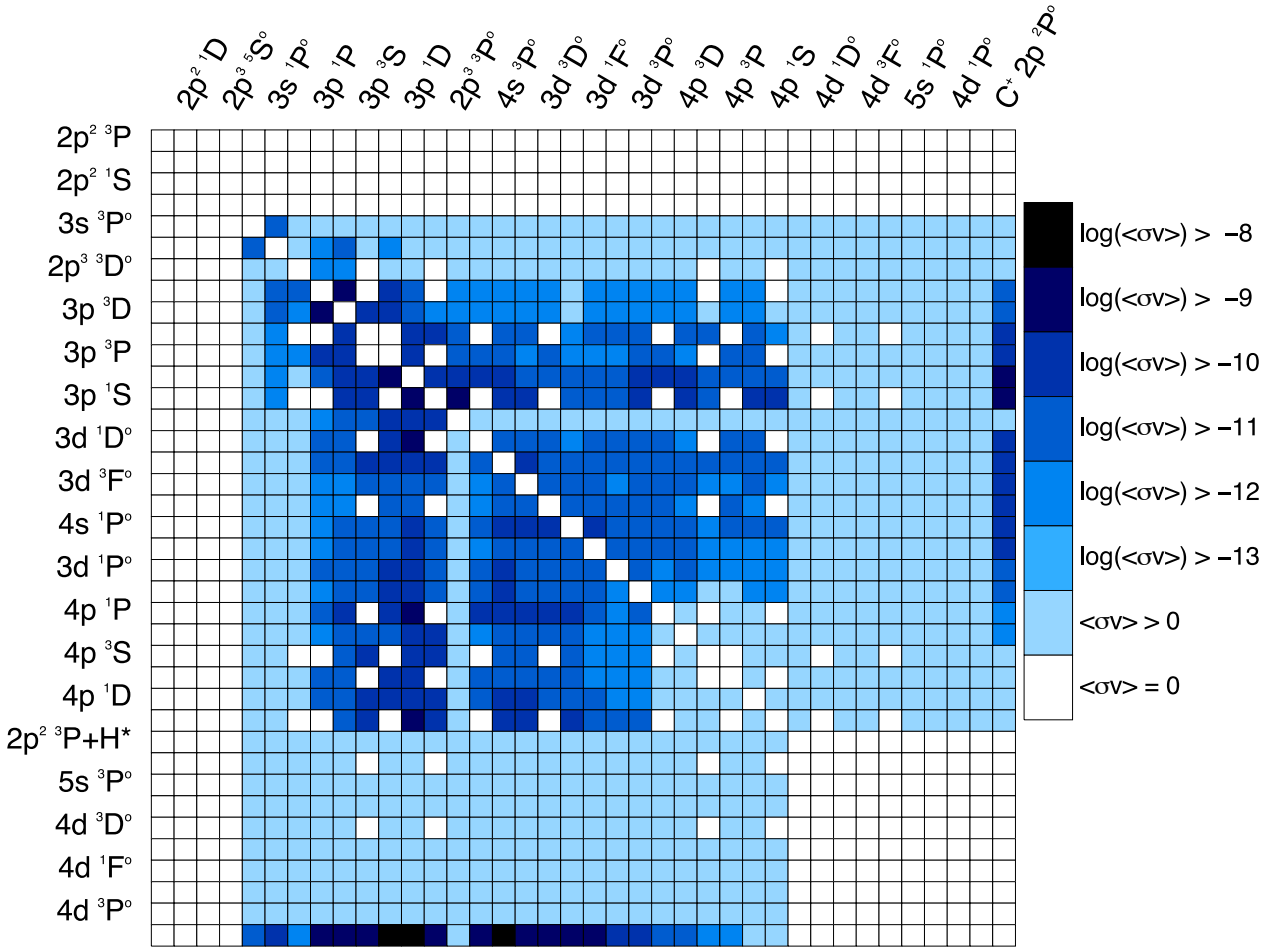

Fig. 3. Graphical representation of the rate coefficient matrices $\langle \sigma v \rangle$ at 6000 K for C+H. Rows give initial states, columns give final states, in order of increasing covalent energies, with every other state being labelled on each axis. The rate coefficients are in $\mathrm{cm^3\ s^{-1}}$.

understood by noting that in the current model, charge transfer corresponds to a single event, of an electron moving from the carbon or nitrogen atom, onto the hydrogen atom (or vice versa). In contrast, excitation requires a second event: that electron moving back onto the carbon or nitrogen atom in some different energy state.

The covalent states involving excited hydrogen, namely C I $2s^2.2p^2\ ^3P + H\,(n = 2)$, and N I $2s^2.2p^3\ ^4S^o/^2D^o + H\,(n = 2)$, correspond to the twenty-ninth row and column of Fig. 3, and the fourth and fifteenth rows and columns of Fig. 4, respectively. For the C I state, the rate coefficients are small ($\langle \sigma v \rangle < 10^{-13}\,\mathrm{cm^3\ s^{-1}}$), owing to the avoided ionic crossing occurring at large internuclear distance (around $80\,a_0$, as mentioned above). Concerning the N I states, however, there are larger rates, between the ground state and the N I $2s^2.2p^2.3s\ ^4P$ state (row 4 – column 5); as well as between the first excited state and the N I $2s^2.2p^2.3p\ ^4S^o/^2D^o/^2P^o$ states (row 15 – columns 11/12/13). In the context of non-LTE stellar spectroscopy, these collisional processes are potentially important: the N I 3s and 3p states give rise to a number of optical and infra-red transitions (see for example Table 2 of Grevesse et al. 1990); then, in so far as N I lines drive the departures from LTE, these collisional processes would have a direct impact on the overall statistical equilibrium.

The C I $2s.2p^3\ ^5S^o/^3D^o/^3P^o$ states, and the N I $2s.2p^4\ ^3D$ state, enter into the model only via two-electron processes involving ground-state hydrogen. They correspond to the fourth, seventh, and fourteenth rows and columns of Fig. 3, and the seventh row and column of Fig. 4, respectively. The rate coefficients involving the C I $2s.2p^3\ ^5S^o$ state are all zero, because no avoided ionic crossings are predicted at these internuclear distances, as mentioned above. For the other states, the figures show that the transitions are generally non-zero. Their rate coefficients are generally smaller (by around a factor of ten) than those of single-electron transitions of similar excitation potentials and transition energies. Nevertheless they can still reach moderately high values ($\langle \sigma v \rangle > 10^{-10}\,\mathrm{cm^3\ s^{-1}}$). Thus, in the context of non-LTE stellar spectroscopy, these collisional processes are also potentially important. However, as we discussed in Sect. 2.1, our current implementation is not ideal, with rough approximations made for the two-electron coupling probability, and the angular momentum couplings, binding energies, and coefficients of fractional parentage of the covalent states. If these transitions are confirmed to be influential on the statistical equilibrium in stellar atmospheres, these calculations should be revisited in a future work.

Lastly, the (mostly blank) fourteenth row and column in Fig. 4 corresponds to the N I $2s^2.2p^2.3s\ ^2D$ state. This state couples to the excited ionic core $N^+\ 2p^2\ ^1D$, and the current model predicts an efficient charge transfer process. This state is also coupled to the low-energy N I $2s^2.2p^3\ ^2D^o$ state, albeit inefficiently, via a two-electron process involving excited hydrogen.

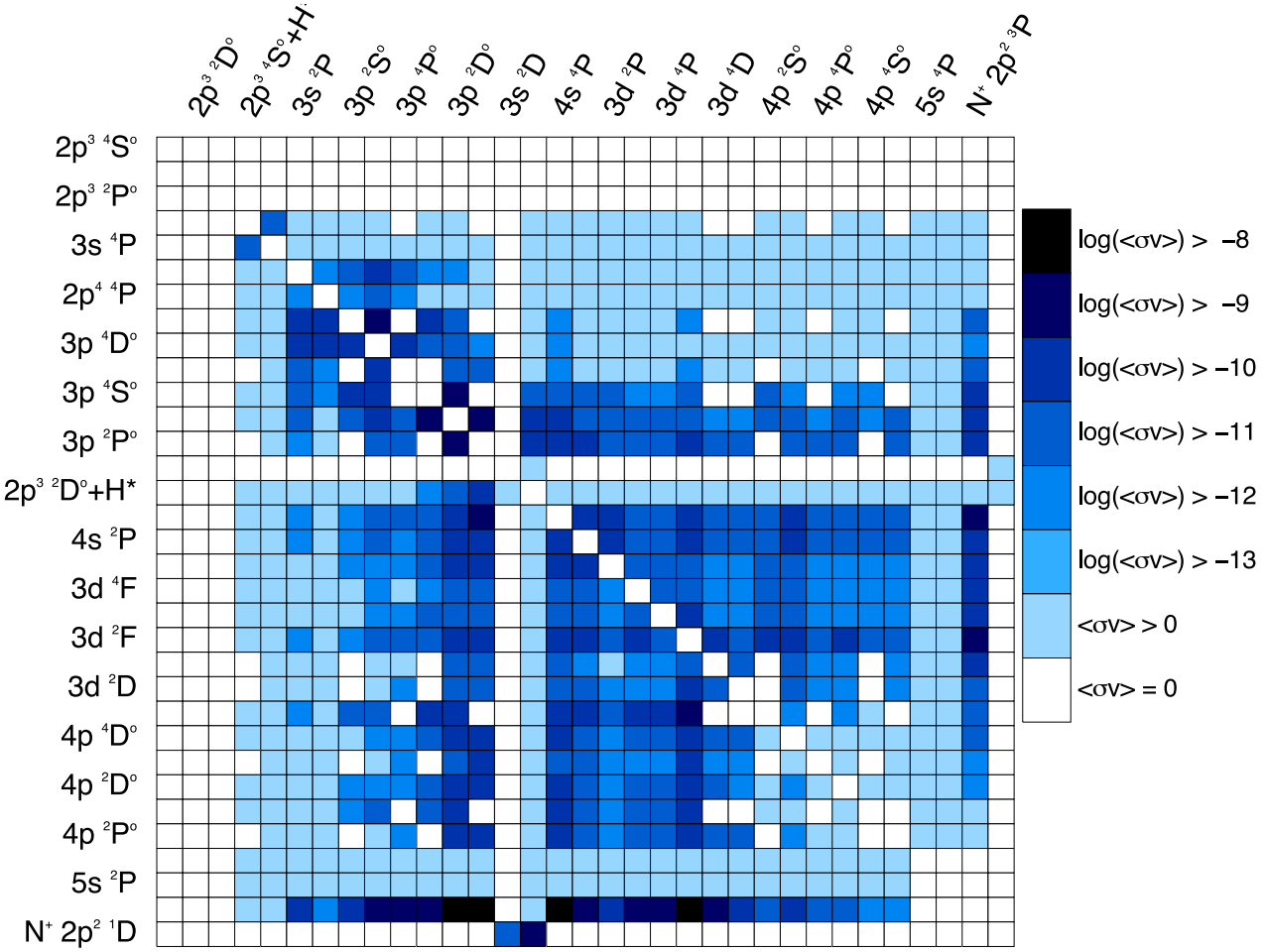

Fig. 4. Graphical representation of the rate coefficient matrices $\langle \sigma v \rangle$ at 6000 K for N+H. Rows give initial states, columns give final states, in order of increasing covalent energies, with every other state being labelled on each axis. The rate coefficients are in $cm^3\ s^{-1}$.

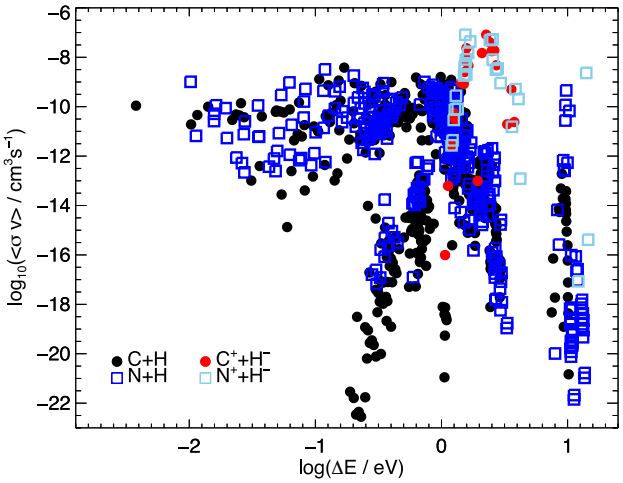

Fig. 5. De-excitation and mutual neutralisation rate coefficients $\langle \sigma v \rangle$ at 6000 K for C+H and N+H.

4. Conclusion

We have presented new calculations for inelastic collisions with neutral hydrogen, for C I and N I, using the LCAO model of Barklem (2016a). This is based on more realistic physics than the approaches commonly used for these species in the current non-LTE literature, including for example the recipe of Drawin (1968, 1969). The rate coefficients for excitation and charge transfer can be found online[2].

Based on earlier work where comparisons could be done with full quantum calculations, as well as indications from calculations using alternate couplings (Barklem 2016a), the uncertainties for the largest rates from these LCAO calculations are expected to be about one order of magnitude, with uncertainties becoming progressively larger as the rates become smaller. As discussed above, transitions involving two-electron processes will have larger uncertainties than those involving one-electron processes, and the results presented here based on two-electron processes should at present only be considered indicative; these processes should be studied more carefully in a future work.

We caution that there is some empirical evidence that the avoided ionic crossing mechanism considered in this work, may not always be the dominant one, and thus that the LCAO results presented here may underestimate the total rate coefficients, for some transitions. In earlier work, using the LCAO results alone that are presented in this work and in Barklem (2018b), we found that the centre-to-limb variations of lines of C I (Amarsi et al. 2019) and O I (Amarsi et al. 2018), precisely observed across the Sun, could not be reproduced by our best models of the solar spectrum.

While this failure could be due to deficiencies in our adopted three-dimensional (3D) hydrodynamic model solar atmosphere

[2] At the CDS and at https://github.com/barklem/public-data

or 3D non-LTE radiative transfer, a possible explanation is that the total O+H and C+H inelastic rate coefficients were being underestimated. In order to reproduce the observations, the LCAO rate coefficients were supplemented, using the free electron formulation of Kaulakys (1985, 1986, 1991). This method considers an alternative mechanism, whereby inelastic processes take place via direct energy and momentum transfer of the (free) active electron on the perturber (as opposed to via electron transfer in the LCAO model). A caveat is that this free electron formulation is strictly valid only in the Rydberg-limit. In summary, further research is still needed into the possible importance of additional mechanisms, including alternative ionic channels.

Acknowledgements. The authors wish to thank the anonymous referee for helpful feedback on the original manuscript. AMA acknowledges funds from the Alexander von Humboldt Foundation in the framework of the Sofja Kovalevskaja Award endowed by the Federal Ministry of Education and Research. PSB acknowledges support from the Swedish Research Council and the project grant "The New Milky Way" from the Knut and Alice Wallenberg Foundation.

References

Adelman, S. A., & Herschbach, D. R. 1977, Mol. Phys., 33, 793
Amarsi, A. M., Barklem, P. S., Asplund, M., Collet, R., & Zatsarinny, O. 2018, A&A, 616, A89
Amarsi, A. M., Barklem, P. S., Collet, R., Grevesse, N., & Asplund, M. 2019, A&A, 624, A111
Asplund, M., Grevesse, N., Sauval, A. J., & Scott, P. 2009, ARA&A, 47, 481
Barklem, P. S. 2016a, Phys. Rev. A, 93, 042705
Barklem, P. S. 2016b, A&ARv, 24, 9
Barklem, P. S. 2018a, A&A, 612, A90
Barklem, P. S. 2018b, A&A, 610, A57
Belyaev, A. K. 1993, Phys. Rev. A, 48, 4299
Belyaev, A. K. 2013, Phys. Rev. A, 88, 052704
Belyaev, A. K., & Barklem, P. S. 2003, Phys. Rev. A, 68, 062703
Belyaev, A. K., & Voronov, Y. V. 2017, A&A, 606, A106
Belyaev, A. K., & Yakovleva, S. A. 2017, A&A, 606, A147
Belyaev, A. K., Grosser, J., Hahne, J., & Menzel, T. 1999, Phys. Rev. A, 60, 2151
Belyaev, A. K., Barklem, P. S., Dickinson, A. S., & Gadéa, F. X. 2010, Phys. Rev. A, 81, 032706
Belyaev, A. K., Barklem, P. S., Spielfiedel, A., et al. 2012, Phys. Rev. A, 85, 032704
Caffau, E., Maiorca, E., Bonifacio, P., et al. 2009, A&A, 498, 877
Caffau, E., Ludwig, H.-G., Bonifacio, P., et al. 2010, A&A, 514, A92
Clegg, R. E. S., Lambert, D. L., & Tomkin, J. 1981, ApJ, 250, 262
Drawin, H.-W. 1968, Z. Phys., 211, 404
Drawin, H. W. 1969, Z. Phys., 225, 483
Ezzeddine, R., Merle, T., Plez, B., et al. 2018, A&A, 618, A141
Gratton, R. G., Sneden, C., Carretta, E., & Bragaglia, A. 2000, A&A, 354, 169
Gratton, R. G., Carretta, E., & Bragaglia, A. 2012, A&ARv, 20, 50
Grevesse, N., Lambert, D. L., Sauval, A. J., et al. 1990, A&A, 232, 225
Grice, R., & Herschbach, D. R. 1974, Mol. Phys., 27, 159
Guitou, M., Belyaev, A. K., Barklem, P. S., Spielfiedel, A., & Feautrier, N. 2011, J. Phys. B At. Mol. Phys., 44, 035202
Kaulakys, B. P. 1985, J. Phys. B At. Mol. Phys., 18, L167
Kaulakys, B. P. 1986, JETP, 91, 391
Kaulakys, B. P. 1991, J. Phys. B At. Mol. Phys., 24, L127
Kramida, A., Ralchenko, Yu., Reader, J., & NIST ASD Team 2015, NIST Atomic Spectra Database (ver. 5.3) [Online] Available: http://physics.nist.gov/asd, [2015, November 2], National Institute of Standards and Technology, Gaithersburg, MD
Lyubimkov, L. S., Lambert, D. L., Korotin, S. A., et al. 2011, MNRAS, 410, 1774
Lyubimkov, L. S., Lambert, D. L., Korotin, S. A., Rachkovskaya, T. M., & Poklad, D. B. 2015, MNRAS, 446, 3447
Martig, M., Fouesneau, M., Rix, H.-W., et al. 2016, MNRAS, 456, 3655
Masseron, T., & Gilmore, G. 2015, MNRAS, 453, 1855
Moore, C. E. 1993, in Tables of Spectra of Hydrogen, Carbon, Nitrogen, and Oxygen Atoms and Ions, ed. J. Gallagher (CRC Press)
Olson, R. E., Smith, F. T., & Bauer, E. 1971, Appl. Opt., 10, 1848
Przybilla, N., & Butler, K. 2001, A&A, 379, 955
Przybilla, N., Butler, K., & Kudritzki, R. P. 2001, A&A, 379, 936
Salaris, M., Pietrinferni, A., Piersimoni, A. M., & Cassisi, S. 2015, A&A, 583, A87
Shi, J. R., Zhao, G., & Chen, Y. Q. 2002, A&A, 381, 982
Spite, M., Cayrel, R., Plez, B., et al. 2005, A&A, 430, 655
Takeda, Y. 1994, PASJ, 46, 53
Takeda, Y., & Honda, S. 2005, PASJ, 57, 65
Tomkin, J., & Lambert, D. L. 1978, ApJ, 223, 937
Wang, Y., Zatsarinny, O., & Bartschat, K. 2013, Phys. Rev. A, 87, 012704
Wang, Y., Zatsarinny, O., & Bartschat, K. 2014, Phys. Rev. A, 89, 062714
Yakovleva, S. A., Voronov, Y. V., & Belyaev, A. K. 2016, A&A, 593, A27
Yakovleva, S. A., Barklem, P. S., & Belyaev, A. K. 2018, MNRAS, 473, 3810

Appendix A: Input data and symmetries considered

Table A.1. Input data for the C+H calculations, sorted by the energies of the covalent CH states, $E_{\mathrm{cov.}}$.

Index	State (A + H)	S_{A}	L_{A}	P_{A}	n_{A}	l_{A}	N_{A}	E_{A}/eV	$E_{\mathrm{cov.}}$/eV	$E_{\mathrm{lim.}}$/eV	Core (C)	$\lvert G^{S_{\mathrm{C}},L_{\mathrm{C}}}_{S_{\mathrm{A}},L_{\mathrm{A}}}\rvert$
1	$2p^2\,{}^3P$	1.0	1	0	2	1	2	0.003667	0.003667	11.265805	$C^+\,2p\,{}^2P^*$	1.0000
2	$2p^2\,{}^1D$	0.0	2	0	2	1	2	1.263725	1.263725	11.265805	$C^+\,2p\,{}^2P^*$	1.0000
3	$2p^2\,{}^1S$	0.0	0	0	2	1	2	2.684011	2.684011	11.265805	$C^+\,2p\,{}^2P^*$	1.0000
4	$2p^3\,{}^5S^o$	2.0	0	1	2	1	3	4.182632	4.182632	16.596210	$C^+\,2p\,{}^2P^*$	1.0000
5	$3s\,{}^3P^o$	1.0	1	1	3	0	1	7.485298	7.485298	11.265805	$C^+\,2p\,{}^2P^*$	1.0000
6	$3s\,{}^1P^o$	0.0	1	1	3	0	1	7.684766	7.684766	11.265805	$C^+\,2p\,{}^2P^*$	1.0000
7	$2p^3\,{}^3D^o$	1.0	2	1	2	1	3	7.946004	7.946004	20.550571	$C^+\,2p\,{}^2P^*$	1.0000
8	$3p\,{}^1P$	0.0	1	0	3	1	1	8.537097	8.537097	11.265805	$C^+\,2p\,{}^2P^*$	1.0000
9	$3p\,{}^3D$	1.0	2	0	3	1	1	8.644426	8.644426	11.265805	$C^+\,2p\,{}^2P^*$	1.0000
10	$3p\,{}^3S$	1.0	0	0	3	1	1	8.771132	8.771132	11.265805	$C^+\,2p\,{}^2P^*$	1.0000
11	$3p\,{}^3P$	1.0	1	0	3	1	1	8.849360	8.849360	11.265805	$C^+\,2p\,{}^2P^*$	1.0000
12	$3p\,{}^1D$	0.0	2	0	3	1	1	9.002582	9.002582	11.265805	$C^+\,2p\,{}^2P^*$	1.0000
13	$3p\,{}^1S$	0.0	0	0	3	1	1	9.171844	9.171844	11.265805	$C^+\,2p\,{}^2P^*$	1.0000
14	$2p^3\,{}^3P^o$	1.0	1	1	2	1	3	9.330422	9.330422	16.596210	$C^+\,2p\,{}^2P^*$	1.0000
15	$3d\,{}^1D^o$	0.0	2	1	3	2	1	9.631070	9.631070	11.265805	$C^+\,2p\,{}^2P^*$	1.0000
16	$4s\,{}^3P^o$	1.0	1	1	4	0	1	9.687238	9.687238	11.265805	$C^+\,2p\,{}^2P^*$	1.0000
17	$3d\,{}^3F^o$	1.0	3	1	3	2	1	9.698831	9.698831	11.265805	$C^+\,2p\,{}^2P^*$	1.0000
18	$3d\,{}^3D^o$	1.0	2	1	3	2	1	9.709173	9.709173	11.265805	$C^+\,2p\,{}^2P^*$	1.0000
19	$4s\,{}^1P^o$	0.0	1	1	4	0	1	9.712957	9.712957	11.265805	$C^+\,2p\,{}^2P^*$	1.0000
20	$3d\,{}^1F^o$	0.0	3	1	3	2	1	9.736432	9.736432	11.265805	$C^+\,2p\,{}^2P^*$	1.0000
21	$3d\,{}^1P^o$	0.0	1	1	3	2	1	9.761433	9.761433	11.265805	$C^+\,2p\,{}^2P^*$	1.0000
22	$3d\,{}^3P^o$	1.0	1	1	3	2	1	9.833789	9.833789	11.265805	$C^+\,2p\,{}^2P^*$	1.0000
23	$4p\,{}^1P$	0.0	1	0	4	1	1	9.988520	9.988520	11.265805	$C^+\,2p\,{}^2P^*$	1.0000
24	$4p\,{}^3D$	1.0	2	0	4	1	1	10.019545	10.019545	11.265805	$C^+\,2p\,{}^2P^*$	1.0000
25	$4p\,{}^3S$	1.0	0	0	4	1	1	10.055742	10.055742	11.265805	$C^+\,2p\,{}^2P^*$	1.0000
26	$4p\,{}^3P$	1.0	1	0	4	1	1	10.084161	10.084161	11.265805	$C^+\,2p\,{}^2P^*$	1.0000
27	$4p\,{}^1D$	0.0	2	0	4	1	1	10.138162	10.138162	11.265805	$C^+\,2p\,{}^2P^*$	1.0000
28	$4p\,{}^1S$	0.0	0	0	4	1	1	10.197912	10.197912	11.265805	$C^+\,2p\,{}^2P^*$	1.0000
29	$2p^2\,{}^3P + H\,(n = 2)$	1.0	1	0	2	1	2	0.003667	10.202497	11.265805	$C^+\,2p\,{}^2P^*$	1.0000
30	$4d\,{}^1D^o$	0.0	2	1	4	2	1	10.352385	10.352385	11.265805	$C^+\,2p\,{}^2P^*$	1.0000
31	$5s\,{}^3P^o$	1.0	1	1	5	0	1	10.386466	10.386466	11.265805	$C^+\,2p\,{}^2P^*$	1.0000
32	$4d\,{}^3F^o$	1.0	3	1	4	2	1	10.386646	10.386646	11.265805	$C^+\,2p\,{}^2P^*$	1.0000
33	$4d\,{}^3D^o$	1.0	2	1	4	2	1	10.394774	10.394774	11.265805	$C^+\,2p\,{}^2P^*$	1.0000
34	$5s\,{}^1P^o$	0.0	1	1	5	0	1	10.404229	10.404229	11.265805	$C^+\,2p\,{}^2P^*$	1.0000
35	$4d\,{}^1F^o$	0.0	3	1	4	2	1	10.413529	10.413529	11.265805	$C^+\,2p\,{}^2P^*$	1.0000
36	$4d\,{}^1P^o$	0.0	1	1	4	2	1	10.418988	10.418988	11.265805	$C^+\,2p\,{}^2P^*$	1.0000
37	$4d\,{}^3P^o$	1.0	1	1	4	2	1	10.428242	10.428242	11.265805	$C^+\,2p\,{}^2P^*$	1.0000
								Ionic states				
38	$2p\,{}^2P^o$	0.5	1	1	2	1	1	11.265805	–	–	–	–

Notes. Unless indicated, ground state hydrogen, H ($n = 1$), is implied. Note that for the $2p^3\,{}^5S^*/{}^3D^*/{}^3P^*$ states the binding energy of the valence electron, $E_{\mathrm{lim.}}$, does not correspond to the energy of the target core; these states are included in the model via two-electron processes involving ground state hydrogen, as discussed in the text.

Table A.2. Input data for the N+H calculations, sorted by the energies of the covalent NH states, $E_{\rm cov.}$.

Index	State (A + H)	$S_{\rm A}$	$L_{\rm A}$	$P_{\rm A}$	$n_{\rm A}$	$l_{\rm A}$	$N_{\rm A}$	$E_{\rm A}$/eV	$E_{\rm cov.}$/eV	$E_{\rm lim.}$/eV	Core (C)	$\lvert G^{S_{\rm C},L_{\rm C}}_{S_{\rm A},L_{\rm A}}\rvert$
1	$2p^3\ ^4S^o$	1.5	0	1	2	1	3	0.000000	0.000000	14.545154	$N^+\ 2p^2\ ^3P$	1.0000
2	$2p^3\ ^2D^o$	0.5	2	1	2	1	3	2.383950	2.383950	14.545154	$N^+\ 2p^2\ ^3P$	0.7071
3	$2p^3\ ^2D^o$	0.5	2	1	2	1	3	2.383950	2.383950	16.433100	$N^+\ 2p^2\ ^1D$	0.7071
4	$2p^3\ ^2P^o$	0.5	1	1	2	1	3	3.575604	3.575604	14.545154	$N^+\ 2p^2\ ^3P$	0.7071
5	$2p^3\ ^2P^o$	0.5	1	1	2	1	3	3.575604	3.575604	16.433100	$N^+\ 2p^2\ ^1D$	0.5270
6	$2p^3\ ^4S^o$ + H ($n = 2$)	1.5	0	1	2	1	3	0.000000	10.198829	14.545154	$N^+\ 2p^2\ ^3P$	1.0000
7	$3s\ ^4P$	1.5	1	0	3	0	1	10.332535	10.332535	14.545154	$N^+\ 2p^2\ ^3P$	1.0000
8	$3s\ ^2P$	0.5	1	0	3	0	1	10.686888	10.686888	14.545154	$N^+\ 2p^2\ ^3P$	1.0000
9	$2p^4\ ^4P$	1.5	1	0	2	1	4	10.926844	10.926844	25.970992	$N^+\ 2p^2\ ^3P$	1.0000
10	$2p^4\ ^4P$	1.5	1	0	2	1	4	10.926844	10.926844	25.970992	$N^+\ 2p^2\ ^1D$	1.0000
11	$3p\ ^2S^o$	0.5	0	1	3	1	1	11.602633	11.602633	14.545154	$N^+\ 2p^2\ ^3P$	1.0000
12	$3p\ ^4D^o$	1.5	2	1	3	1	1	11.758641	11.758641	14.545154	$N^+\ 2p^2\ ^3P$	1.0000
13	$3p\ ^4P^o$	1.5	1	1	3	1	1	11.841881	11.841881	14.545154	$N^+\ 2p^2\ ^3P$	1.0000
14	$3p\ ^4S^o$	1.5	0	1	3	1	1	11.995575	11.995575	14.545154	$N^+\ 2p^2\ ^3P$	1.0000
15	$3p\ ^2D^o$	0.5	2	1	3	1	1	12.005929	12.005929	14.545154	$N^+\ 2p^2\ ^3P$	1.0000
16	$3p\ ^2P^o$	0.5	1	1	3	1	1	12.125052	12.125052	14.545154	$N^+\ 2p^2\ ^3P$	1.0000
17	$3s\ ^2D$	0.5	2	0	3	0	1	12.356713	12.356713	16.433100	$N^+\ 2p^2\ ^1D$	1.0000
18	$2p^3\ ^2D^o$ + H ($n = 2$)	0.5	2	1	2	1	3	2.383950	12.582779	14.545154	$N^+\ 2p^2\ ^3P$	0.7071
19	$2p^3\ ^2D^o$ + H ($n = 2$)	0.5	2	1	2	1	3	2.383950	12.582779	16.433100	$N^+\ 2p^2\ ^1D$	0.7071
20	$4s\ ^4P$	1.5	1	0	4	0	1	12.856736	12.856736	14.545154	$N^+\ 2p^2\ ^3P$	1.0000
21	$4s\ ^2P$	0.5	1	0	4	0	1	12.918978	12.918978	14.545154	$N^+\ 2p^2\ ^3P$	1.0000
22	$3d\ ^2P$	0.5	1	0	3	2	1	12.972099	12.972099	14.545154	$N^+\ 2p^2\ ^3P$	1.0000
23	$3d\ ^4F$	1.5	3	0	3	2	1	12.983688	12.983688	14.545154	$N^+\ 2p^2\ ^3P$	1.0000
24	$3d\ ^4P$	1.5	1	0	3	2	1	12.999168	12.999168	14.545154	$N^+\ 2p^2\ ^3P$	1.0000
25	$3d\ ^2F$	0.5	3	0	3	2	1	12.999906	12.999906	14.545154	$N^+\ 2p^2\ ^3P$	1.0000
26	$3d\ ^4D$	1.5	2	0	3	2	1	13.019322	13.019322	14.545154	$N^+\ 2p^2\ ^3P$	1.0000
27	$3d\ ^2D$	0.5	2	0	3	2	1	13.035010	13.035010	14.545154	$N^+\ 2p^2\ ^3P$	1.0000
28	$4p\ ^2S^o$	0.5	0	1	4	1	1	13.201565	13.201565	14.545154	$N^+\ 2p^2\ ^3P$	1.0000
29	$4p\ ^4D^o$	1.5	2	1	4	1	1	13.244657	13.244657	14.545154	$N^+\ 2p^2\ ^3P$	1.0000
30	$4p\ ^4P^o$	1.5	1	1	4	1	1	13.268207	13.268207	14.545154	$N^+\ 2p^2\ ^3P$	1.0000
31	$4p\ ^2D^o$	0.5	2	1	4	1	1	13.294300	13.294300	14.545154	$N^+\ 2p^2\ ^3P$	1.0000
32	$4p\ ^4S^o$	1.5	0	1	4	1	1	13.321559	13.321559	14.545154	$N^+\ 2p^2\ ^3P$	1.0000
33	$4p\ ^2P^o$	0.5	1	1	4	1	1	13.342725	13.342725	14.545154	$N^+\ 2p^2\ ^3P$	1.0000
34	$5s\ ^4P$	1.5	1	0	5	0	1	13.624243	13.624243	14.545154	$N^+\ 2p^2\ ^3P$	1.0000
35	$5s\ ^2P$	0.5	1	0	5	0	1	13.648602	13.648602	14.545154	$N^+\ 2p^2\ ^3P$	1.0000
								Ionic states				
36	$N^+\ 2p^2\ ^3P$	1.0	1	0	2	1	2	14.545154	–	–	–	–
37	$N^+\ 2p^2\ ^1D$	0.0	2	0	2	1	2	16.433100	–	–	–	–

Notes. Unless indicated, ground state hydrogen, H ($n = 1$), is implied. Note that for the $2s.2p^4\ ^3D$ state the binding energy of the valence electron, $E_{\rm lim.}$, does not correspond to the energy of the target core; these states are included in the model via two-electron processes involving ground state hydrogen, as discussed in the text.

Table A.3. Possible symmetries for the CH molecular states.

Index	State	g_{total}	Symmetries
1	$2p^2\,{}^3P$	18	$^2\Sigma^-$, $^2\Pi$, $^4\Sigma^-$, $^4\Pi$
2	$2p^2\,{}^1D$	10	$^2\Sigma^+$, $^2\Pi$, $^2\Delta$
3	$2p^2\,{}^1S$	2	$^2\Sigma^+$
4	$2p^3\,{}^5S^o$	10	$^4\Sigma^-$, $^6\Sigma^-$
5	$3s\,{}^3P^o$	18	$^2\Sigma^+$, $^2\Pi$, $^4\Sigma^+$, $^4\Pi$
6	$3s\,{}^1P^o$	6	$^2\Sigma^+$, $^2\Pi$
7	$2p^3\,{}^3D^o$	30	$^2\Sigma^-$, $^2\Pi$, $^2\Delta$, $^4\Sigma^-$, $^4\Pi$, $^4\Delta$
8	$3p\,{}^1P$	6	$^2\Sigma^-$, $^2\Pi$
9	$3p\,{}^3D$	30	$^2\Sigma^+$, $^2\Pi$, $^2\Delta$, $^4\Sigma^+$, $^4\Pi$, $^4\Delta$
10	$3p\,{}^3S$	6	$^2\Sigma^+$, $^4\Sigma^+$
11	$3p\,{}^3P$	18	$^2\Sigma^-$, $^2\Pi$, $^4\Sigma^-$, $^4\Pi$
12	$3p\,{}^1D$	10	$^2\Sigma^+$, $^2\Pi$, $^2\Delta$
13	$3p\,{}^1S$	2	$^2\Sigma^+$
14	$2p^3\,{}^3P^o$	18	$^2\Sigma^+$, $^2\Pi$, $^4\Sigma^+$, $^4\Pi$
15	$3d\,{}^1D^o$	10	$^2\Sigma^-$, $^2\Pi$, $^2\Delta$
16	$4s\,{}^3P^o$	18	$^2\Sigma^+$, $^2\Pi$, $^4\Sigma^+$, $^4\Pi$
17	$3d\,{}^3F^o$	42	$^2\Sigma^+$, $^2\Pi$, $^2\Delta$, $^2\Phi$, $^4\Sigma^+$, $^4\Pi$, $^4\Delta$, $^4\Phi$
18	$3d\,{}^3D^o$	30	$^2\Sigma^-$, $^2\Pi$, $^2\Delta$, $^4\Sigma^-$, $^4\Pi$, $^4\Delta$
19	$4s\,{}^1P^o$	6	$^2\Sigma^+$, $^2\Pi$
20	$3d\,{}^1F^o$	14	$^2\Sigma^+$, $^2\Pi$, $^2\Delta$, $^2\Phi$
21	$3d\,{}^1P^o$	6	$^2\Sigma^+$, $^2\Pi$
22	$3d\,{}^3P^o$	18	$^2\Sigma^+$, $^2\Pi$, $^4\Sigma^+$, $^4\Pi$
23	$4p\,{}^1P$	6	$^2\Sigma^-$, $^2\Pi$
24	$4p\,{}^3D$	30	$^2\Sigma^+$, $^2\Pi$, $^2\Delta$, $^4\Sigma^+$, $^4\Pi$, $^4\Delta$
25	$4p\,{}^3S$	6	$^2\Sigma^+$, $^4\Sigma^+$
26	$4p\,{}^3P$	18	$^2\Sigma^-$, $^2\Pi$, $^4\Sigma^-$, $^4\Pi$
27	$4p\,{}^1D$	10	$^2\Sigma^+$, $^2\Pi$, $^2\Delta$
28	$4p\,{}^1S$	2	$^2\Sigma^+$
29	$2p^2\,{}^3P + H\,(n = 2)$	72	$^2\Sigma^-$, $^2\Pi$, $^4\Sigma^-$, $^4\Pi$, $^2\Sigma^+$, $^2\Delta$, $^4\Sigma^+$, $^4\Delta$
30	$4d\,{}^1D^o$	10	$^2\Sigma^-$, $^2\Pi$, $^2\Delta$
31	$5s\,{}^3P^o$	18	$^2\Sigma^+$, $^2\Pi$, $^4\Sigma^+$, $^4\Pi$
32	$4d\,{}^3F^o$	42	$^2\Sigma^+$, $^2\Pi$, $^2\Delta$, $^2\Phi$, $^4\Sigma^+$, $^4\Pi$, $^4\Delta$, $^4\Phi$
33	$4d\,{}^3D^o$	30	$^2\Sigma^-$, $^2\Pi$, $^2\Delta$, $^4\Sigma^-$, $^4\Pi$, $^4\Delta$
34	$5s\,{}^1P^o$	6	$^2\Sigma^+$, $^2\Pi$
35	$4d\,{}^1F^o$	14	$^2\Sigma^+$, $^2\Pi$, $^2\Delta$, $^2\Phi$
36	$4d\,{}^1P^o$	6	$^2\Sigma^+$, $^2\Pi$
37	$4d\,{}^3P^o$	18	$^2\Sigma^+$, $^2\Pi$, $^4\Sigma^+$, $^4\Pi$
38	$C^+\,2p\,{}^2P^o$	6	$^2\Sigma^+$, $^2\Pi$
Number of symmetries to calculate: 2			$^2\Sigma^+$, $^2\Pi$
g:			2, 4

Table A.4. Possible symmetries for the NH molecular states.

Index	State	$g_{\rm total}$	Symmetries
1	$2p^3\,{}^4S^o$	8	$^3\Sigma^-$, $^5\Sigma^-$
2	$2p^3\,{}^2D^o$	20	$^1\Sigma^-$, $^1\Pi$, $^1\Delta$, $^3\Sigma^-$, $^3\Pi$, $^3\Delta$
3	$2p^3\,{}^2P^o$	12	$^1\Sigma^+$, $^1\Pi$, $^3\Sigma^+$, $^3\Pi$
4	$2p^3\,{}^4S^o + H\,(n = 2)$	32	$^3\Sigma^-$, $^5\Sigma^-$, $^3\Pi$, $^5\Pi$
5	$3s\,{}^4P$	24	$^3\Sigma^-$, $^3\Pi$, $^5\Sigma^-$, $^5\Pi$
6	$3s\,{}^2P$	12	$^1\Sigma^-$, $^1\Pi$, $^3\Sigma^-$, $^3\Pi$
7	$2p^4\,{}^4P$	24	$^3\Sigma^-$, $^3\Pi$, $^5\Sigma^-$, $^5\Pi$
8	$3p\,{}^2S^o$	4	$^1\Sigma^-$, $^3\Sigma^-$
9	$3p\,{}^4D^o$	40	$^3\Sigma^-$, $^3\Pi$, $^3\Delta$, $^5\Sigma^-$, $^5\Pi$, $^5\Delta$
10	$3p\,{}^4P^o$	24	$^3\Sigma^+$, $^3\Pi$, $^5\Sigma^+$, $^5\Pi$
11	$3p\,{}^4S^o$	8	$^3\Sigma^-$, $^5\Sigma^-$
12	$3p\,{}^2D^o$	20	$^1\Sigma^-$, $^1\Pi$, $^1\Delta$, $^3\Sigma^-$, $^3\Pi$, $^3\Delta$
13	$3p\,{}^2P^o$	12	$^1\Sigma^+$, $^1\Pi$, $^3\Sigma^+$, $^3\Pi$
14	$3s\,{}^2D$	20	$^1\Sigma^+$, $^1\Pi$, $^1\Delta$, $^3\Sigma^+$, $^3\Pi$, $^3\Delta$
15	$2p^3\,{}^2D^o + H\,(n = 2)$	80	$^1\Sigma^-$, $^1\Pi$, $^1\Delta$, $^3\Sigma^-$, $^3\Pi$, $^3\Delta$, $^1\Sigma^+$, $^1\Phi$, $^3\Sigma^+$, $^3\Phi$
16	$4s\,{}^4P$	24	$^3\Sigma^-$, $^3\Pi$, $^5\Sigma^-$, $^5\Pi$
17	$4s\,{}^2P$	12	$^1\Sigma^-$, $^1\Pi$, $^3\Sigma^-$, $^3\Pi$
18	$3d\,{}^2P$	12	$^1\Sigma^-$, $^1\Pi$, $^3\Sigma^-$, $^3\Pi$
19	$3d\,{}^4F$	56	$^3\Sigma^-$, $^3\Pi$, $^3\Delta$, $^3\Phi$, $^5\Sigma^-$, $^5\Pi$, $^5\Delta$, $^5\Phi$
20	$3d\,{}^4P$	24	$^3\Sigma^-$, $^3\Pi$, $^5\Sigma^-$, $^5\Pi$
21	$3d\,{}^2F$	28	$^1\Sigma^-$, $^1\Pi$, $^1\Delta$, $^1\Phi$, $^3\Sigma^-$, $^3\Pi$, $^3\Delta$, $^3\Phi$
22	$3d\,{}^4D$	40	$^3\Sigma^+$, $^3\Pi$, $^3\Delta$, $^5\Sigma^+$, $^5\Pi$, $^5\Delta$
23	$3d\,{}^2D$	20	$^1\Sigma^+$, $^1\Pi$, $^1\Delta$, $^3\Sigma^+$, $^3\Pi$, $^3\Delta$
24	$4p\,{}^2S^o$	4	$^1\Sigma^-$, $^3\Sigma^-$
25	$4p\,{}^4D^o$	40	$^3\Sigma^-$, $^3\Pi$, $^3\Delta$, $^5\Sigma^-$, $^5\Pi$, $^5\Delta$
26	$4p\,{}^4P^o$	24	$^3\Sigma^+$, $^3\Pi$, $^5\Sigma^+$, $^5\Pi$
27	$4p\,{}^2D^o$	20	$^1\Sigma^-$, $^1\Pi$, $^1\Delta$, $^3\Sigma^-$, $^3\Pi$, $^3\Delta$
28	$4p\,{}^4S^o$	8	$^3\Sigma^-$, $^5\Sigma^-$
29	$4p\,{}^2P^o$	12	$^1\Sigma^+$, $^1\Pi$, $^3\Sigma^+$, $^3\Pi$
30	$5s\,{}^4P$	24	$^3\Sigma^-$, $^3\Pi$, $^5\Sigma^-$, $^5\Pi$
31	$5s\,{}^2P$	12	$^1\Sigma^-$, $^1\Pi$, $^3\Sigma^-$, $^3\Pi$
32	$N^+\,2p^2\,{}^3P$	9	$^3\Sigma^-$, $^3\Pi$
33	$N^+\,2p^2\,{}^1D$	5	$^1\Sigma^+$, $^1\Pi$, $^1\Delta$
Number of symmetries to calculate: 5			$^3\Sigma^-$, $^3\Pi$, $^1\Sigma^+$, $^1\Pi$, $^1\Delta$
g:			3, 6, 1, 2, 2